Available online at www.sciencedirect.com
ScienceDirect
Bioelectrochemistry 69 (2006) 88–93
Bioelectrochemistry
www.elsevier.com/locate/bioelechem

Three dimensional transport lattice model for describing action potentials in axons stimulated by external electrodes

Donald A. Stewart, T.R. Gowrishankar, James C. Weaver *

Harvard-MIT Division of Health Sciences and Technology, Massachusetts Institute of Technology, Cambridge, MA, USA

Received 6 July 2005; received in revised form 30 September 2005; accepted 7 November 2005
Available online 27 January 2006

Abstract

Conditions that stimulate action potentials in one or more nerves is of widespread interest. Axon and nerve models are usually based on two dimensional pre-specified lumped equivalents that assume where currents will flow. In contrast, here we illustrate creation of three dimensional (3D) system models with a transport lattice of interconnected local models for external and internal electrolyte and axon membrane. The transport lattice solves Laplace's equation in the extracellular medium and is coupled to the Hodgkin–Huxley model at local membrane sites. These space-filling models incorporate the geometric scale, which allows explicit representation of confined axons and external electrodes. The present results demonstrate feasibility of the basic approach. These models are spatially coarse and approximate, but can be straightforwardly improved. The transport lattice system models are modular and multiscale (spatial scales ranging from the membrane thickness of 5 nm to the axon segment length of 2 cm).

Keywords: Transport lattice model; Axon; Action potential; External electrodes; Three dimensional model

1. Introduction

Computational and analytical models that describe the behavior of axons and of myelinated nerves are of long standing interest [1,2] with progressively more realistic features included in models [3–5]. Analytical models with closed form mathematical solutions can also provide useful insights [6,7]. Computer models solved by numerical methods allow increasingly realistic features to be incorporated, such as the functional and topological features of nerves, including branching [8,9]. Examples of systems which have been modeled include neurons [10,11] and spinal cord potentials [12]. Some models use circuit simulation software, such as SPICE [13–17], including models of interactions between electrodes and neurons [18,19]. For example, the present 3D model is an extension of the equivalent circuit modeling approach described by Bunow et al. which assumed cylindrical symmetry of the axon and the stimulus [13].

It has been noted [4,5] that widely used lumped circuit models assume current paths based on relationships between circuit elements, and both neural and extracellular geometry. These models do not allow direct exploration of electrode geometry and the resulting distribution of fields and currents within a nerve bundle. Some recent finite element models [4,5] do indeed use geometry-based models to represent a neuron–electrode interface for the case where the neuron soma is almost sealed to a micro-electrode [20,21].

Our goal is to begin to approach the problem of creating space-filling models of axons and nerves in which geometric structure and quantitative functional models can be added, removed or modified, in order to test hypotheses. The idea is simple: creation of space-filling models which have some, or all, of the essential features that represent a hypothesis. Then, by applying various voltage or current stimuli via two or more electrodes it can be seen whether or not a propagating action potential occurs (an example of a hypothesis test). The basic approach can be straightforwardly expanded to progressively more comprehensive and realistic models.

* Corresponding author. MIT, Rm. 16-319, Cambridge, MA 02139, USA. Tel.: +1 617 253 4194; fax: +1 617 253 2514.
E-mail address: jcw@mit.edu (J.C. Weaver).

1567-5394/$ - see front matter © 2006 Published by Elsevier B.V.
doi:10.1016/j.bioelechem.2005.11.004

2. Methods

We use a transport lattice approach [22–25] to construct a three dimensional system model that contains both cells (here one or two axons), intra- and extracellular aqueous electrolyte, and electrodes that provide stimuli. We demonstrate an elementary space-filling model that intrinsically provides for the heterogeneous stimulation currents that flow from, and into, finite external electrodes that can have their location, size and shape varied.

The single axon system model (Fig. 1) is a Cartesian lattice with spatial dimensions of $[N_x-1]\ell_x \times [N_z-1]\ell_y \times [N_z-1]\ell_z = 20\ \mu m \times 20\ \mu m \times 2$ cm (Table 1). Here N_i is the number of nodes along the indicated axis, and l_i is the corresponding internodal spacing. Between each node is a local transport model which represents either electrolyte (open boxes) or axon membrane sandwiched between electrolyte (hatched boxes). All the intra-nodal transport models in the z-direction are pure electrolyte. The circuit element for these models is a simple resistor: $R_{e,z}=\rho_e \ell_z/\ell_x\ell_y = 0.7$ MΩ. For simplicity, the extracellular electrolyte and the intracellular electrolyte have the same resistivity, ρ_e. In the x and y directions, the local electrolyte transport models are resistors: $R_{e,x}=R_{e,y}=\rho_e \ell_x/\ell_y\ell_z = 7$ KΩ. The local models between nodes spanning axon membrane (hatched boxes) consist of a membrane model sandwiched between two electrolyte models of half thickness ($R_{e,x}/2 = 3.5$ KΩ) as shown in Fig. 2. Although the membrane thickness (5 nm) is much smaller than the lattice spacing (10 μm), the membrane sandwich properly accounts for transmembrane charge transport [22,23]. There is no charge transport within the membrane parallel to the membrane surface. The local membrane model is based on the original Hodgkin–Huxley [26] (HH) model and the equivalent circuit [13], corresponding to the black box in Fig. 2. Parameters for the axon membrane are scaled to the local membrane area ($\ell_x \times \ell_z$) and are listed in Table 1.

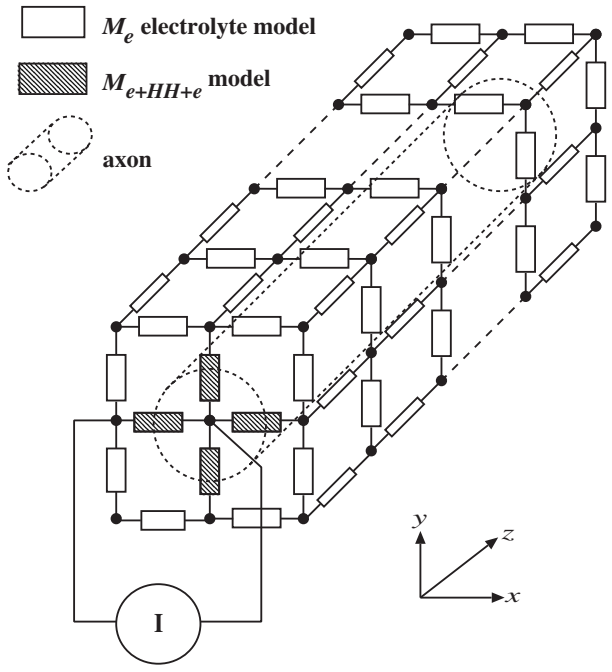

Fig. 1. Single axon system model based on an elongated transport lattice. The system model contains interconnected local models for aqueous electrolytes, local membrane regions with Hodgkin–Huxley (HH) behavior, and point electrodes that provide the current clamp stimulus. This lattice is $3\times3\times200$ nodes in the x, y, and z directions with inter-nodal spacing $\ell_x=\ell_y=10$ μm, and $\ell_z=100$ μm. Extracellular aqueous electrolyte is represented by interconnected resistances, $R_{e,x}=R_{e,y}=\rho_e/\ell_z=7$ KΩ. The longer aqueous pathway segments (internal and external to the axon) in the z direction have magnitude $R_{e,z}=\rho_e\ell_z/\ell_x^2=700$ KΩ.

Table 1
Parameters for system model

Parameter	Description	Value
$N_x\times N_y\times N_z$	Number of nodes in 1 axon system model	$3\times3\times200$
	Number of nodes in 2 axon system model	$7\times7\times25$
$L_x\times L_y\times L_z$	1 axon system model volume	$20\times20\times20\times10^3$ μm^3
	2 axon system model volume	$60\times60\times0.25\times10^3$ μm^3
ℓ_x, ℓ_y	Lattice spacing in x and y	10 μm
ℓ_z	Lattice spacing in z	100 μm
r_a	Effective small axon radius	5 μm
	Effective large axon radius	10 μm
C_m	Membrane specific capacitance	1 μF cm^{-2}
ρ_e	Electrolyte resistivity	0.7 Ω m
T	Temperature	279.3 K
G_{Na}	Sodium channel base conductivity per unit membrane area	1200 mS m^{-2}
G_K	Potassium channel base conductivity per unit membrane area	360 mS m^{-2}
G_L	Leakage base conductivity per unit membrane area	3 mS m^{-2}
V_{Na}	Sodium channel bias voltage	55 mV
V_K	Potassium channel bias voltage	−72 mV
V_L	Membrane bias voltage	−49 mV

A full three dimensional representation of an axon within a system volume allows increased flexibility in simulating electrical stimuli that might trigger a propagating action potential. Fig. 1 shows a single axon in a current clamp configuration. The current clamp is a current source between the inside and outside of the axon at one end of the axon. This system is axially symmetric and could be modeled without the full 3D lattice as described previously [13,27]. Here we use the system model of Fig. 1 to compare with previous models for validation.

Fig. 3 shows a system of two axons exposed to an electric field. The electric field is created by a voltage source connected across lines of nodes along the boundary to simulate a pair of needle electrodes of diameter ~0.1 mm. This system has insufficient symmetry to be modeled without a full 3D lattice. The system model of Fig. 3 is a 60 μm × 60 μm × 2.5 mm region segmented into a lattice of $7\times7\times25$ nodes. The axis of each axon runs along the z direction. One axon has a small cross section (only one line of nodes inside the axon membrane) and the other has a cross section four times larger. The effective radius is roughly $r_a=\ell_x/2=5$ μm for the small axon, and 10 μm for the larger axon in the two axon system model. The system consisting of two axons and surrounding electrolyte is exposed to an electric field pulse, of amplitudes ranging from $V=50$ to

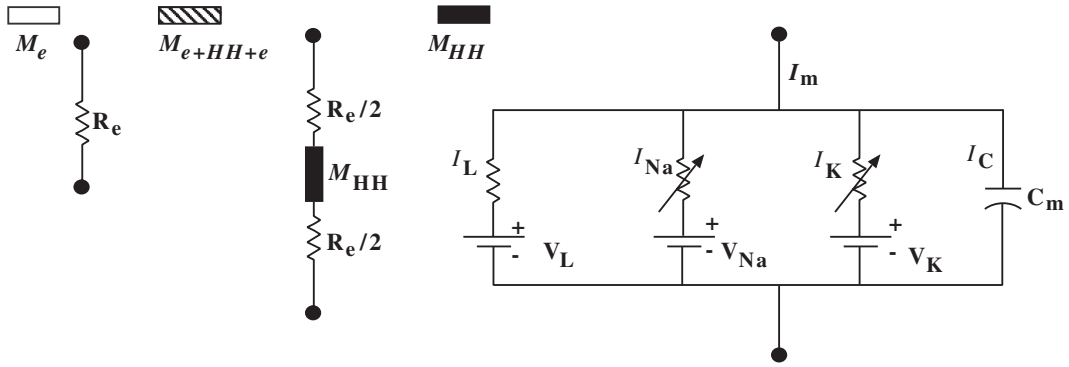

Fig. 2. Electrolyte and membrane–electrolyte interface local models. The extracellular electrolyte and cytoplasm are represented by local models, M_e. The intranodal model spanning axon membrane (M_{e+HH+e}) is a thin membrane model (M_{HH}) sandwiched between two electrolyte models of half thickness. The M_{HH} membrane model has the Hodgkin–Huxley representation of Sodium ($I_{Na}=\ell_x\times\ell_z\cdot G_{Na}m^3h(U_m-V_{Na})$), Potassium ($I_K=\ell_x\times\ell_z\cdot G_K n^4(U_m-V_K)$) ion channels, leakage current ($I_L=\ell_x\times\ell_z\cdot G_L(U_m-V_L)$, and membrane displacement current ($I_C=\ell_x\times\ell_z\cdot C_m dU_m/dt$). Standard values for the conductivities and resting potentials were used: $G_{Na}=120$ mS/cm^2, $G_K=36$ mS/cm^2, $G_L=0.3$ mS/cm^2, $V_{Na}=55$ mV, $V_K=-72$ mV, $V_L=-49$ mV, $C_m=1$ μF/cm^2. The model implicitly includes the differential equations for the activation parameters n, m, and h [1]. These local currents scale with the local (elemental) membrane area $\ell_x\times\ell_z=10^{-9}$ m^2 (here $\ell_x=\ell_y$).

1500 mV across the system volume. The pulse duration is 0.5 ms with zero rise and fall time. Voltage pulses across the electrodes at the side of the system model volume as shown in Fig. 3 generates an applied electric field ($E=V/60$ μm)) from $E=8.3$ to 117 V cm^{-1} at $z=0$ with a fringe field extending out in z. The resulting action potentials, or lack thereof, in response to the E field stimulus are then observed propagating along the z axis.

The transport lattice method employs locally interacting functional models (Fig. 2) that describe charge transport in aqueous electrolytes and non-linear in which the HH parameters are scaled to Hodgkin–Huxley model of membrane. The

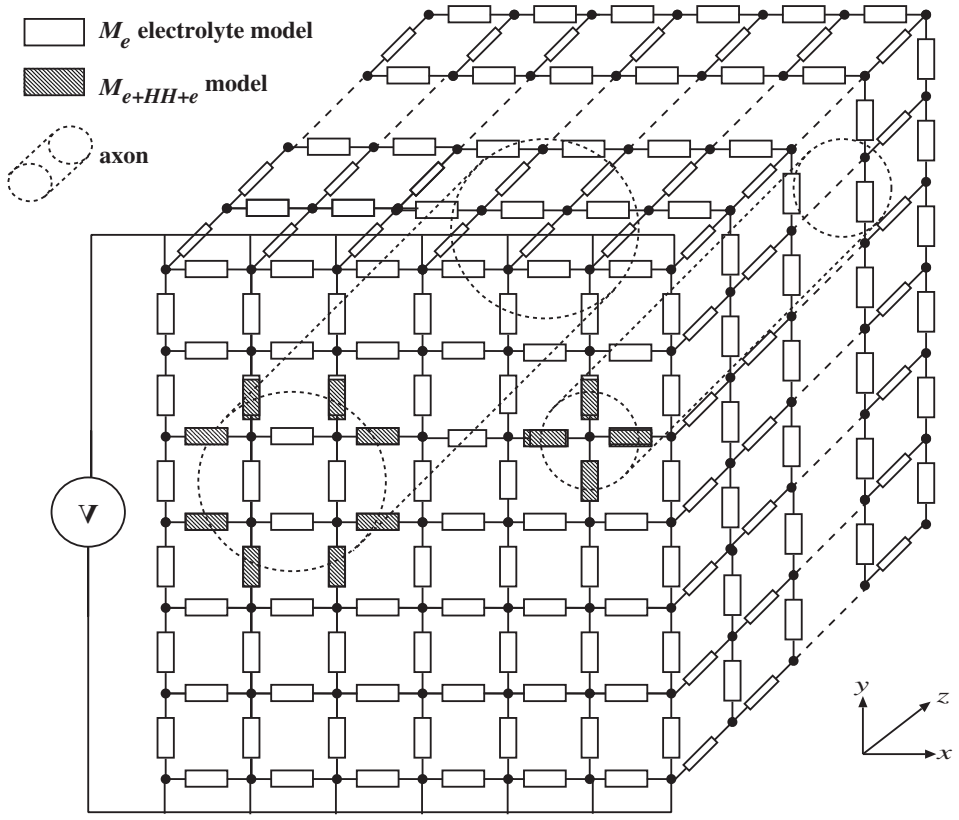

Fig. 3. Two axon transport lattice system model. The system model consists of a Cartesian lattice with $7\times7\times25$ nodes in the x, y, and z directions, with the nodes separated by $\ell_x=\ell_y=10$ μm in the x and y directions and by $\ell_z=100$ μm in the z direction. Each axon membrane is represented by a Hodgkin–Huxley model (Fig. 2) that connects two aqueous electrolyte regions (intra- and extracellular electrolyte). The many interconnected local electrolyte models allow fields and currents to approximately satisfy Laplace's equation within the extracellular region [22]. The model's response is computed by solving the corresponding three dimensional circuit using SPICE, which solves for the transient voltage at each node in response to a voltage pulse. The application electrodes are vertical lines of nodes on opposing sides of the volume at $z=0$.

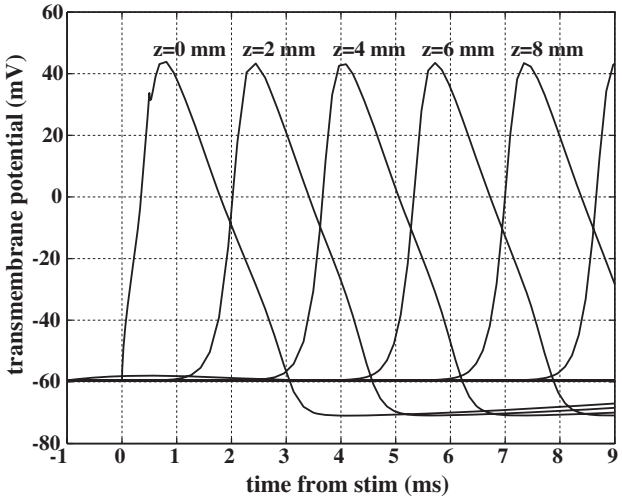

Fig. 4. Propagating action potential from a current clamp stimulus. In a current clamp, the stimulus is a current across the axon membrane (one electrode inside the axon and the other outside). The stimulus of 20 nA starts at $t=0$ and ends at $t=0.5$ ms. The propagating action potential, seen here as a transmembrane potential wave, is triggered by the current clamp stimulus and travels down the length of the axon. The action potential rises to a peak voltage of 43 mV before returning to a resting potential of −59 mV.

resulting electrical circuits are solved by Kirchhoff's laws using Berkeley SPICE version 3f5 [28,29], yielding currents and voltages of lattice elements. Matlab (MathWorks, Natick, MA) is used to generate the SPICE input file and process and display the output voltages and currents. A Pentium based computer (2 GHz CPU, 4 GB RAM) was used to obtain the solutions. Typical processing times were 2 min per simulation.

3. Results and discussion

Fig. 4 shows solutions of the current clamp model of Fig. 1 as time dependent transmembrane potentials, $U_m(z,t)$ in response to a current stimulus at $z=0$ of amplitude 20 μA/mm^2 and duration 0.5 ms. Several slices along the axon axis (z direction) are plotted and labeled at the waveform peak. The action potential of U_m rises from the resting potential of the axon of −59 mV to a peak of 43.5 mV in 1.5 ms and then falls to −71 mV in 3 ms before recovering back to the resting potential with a time constant of roughly 10 ms. The propagation speed of the action potential is 1.20±0.02 m s^{-1}. This result can be benchmarked against existing numerical tools. The waveform amplitude, shape, and propagation speed shown in Fig. 4 are all in good agreement (within 1% using parameters listed in Table 1) to results from a Finite Element toolkit developed for a quantitative physiology course at MIT [1,27].

Fig. 5 shows transmembrane potentials for the two axon system model (Fig. 3) exposed to applied electric field pulses. The panels correspond to a range of applied electric fields from 8.3 V cm^{-1} ($V=50$ mV) to 117 V cm^{-1} ($V=0.7$ V) and show

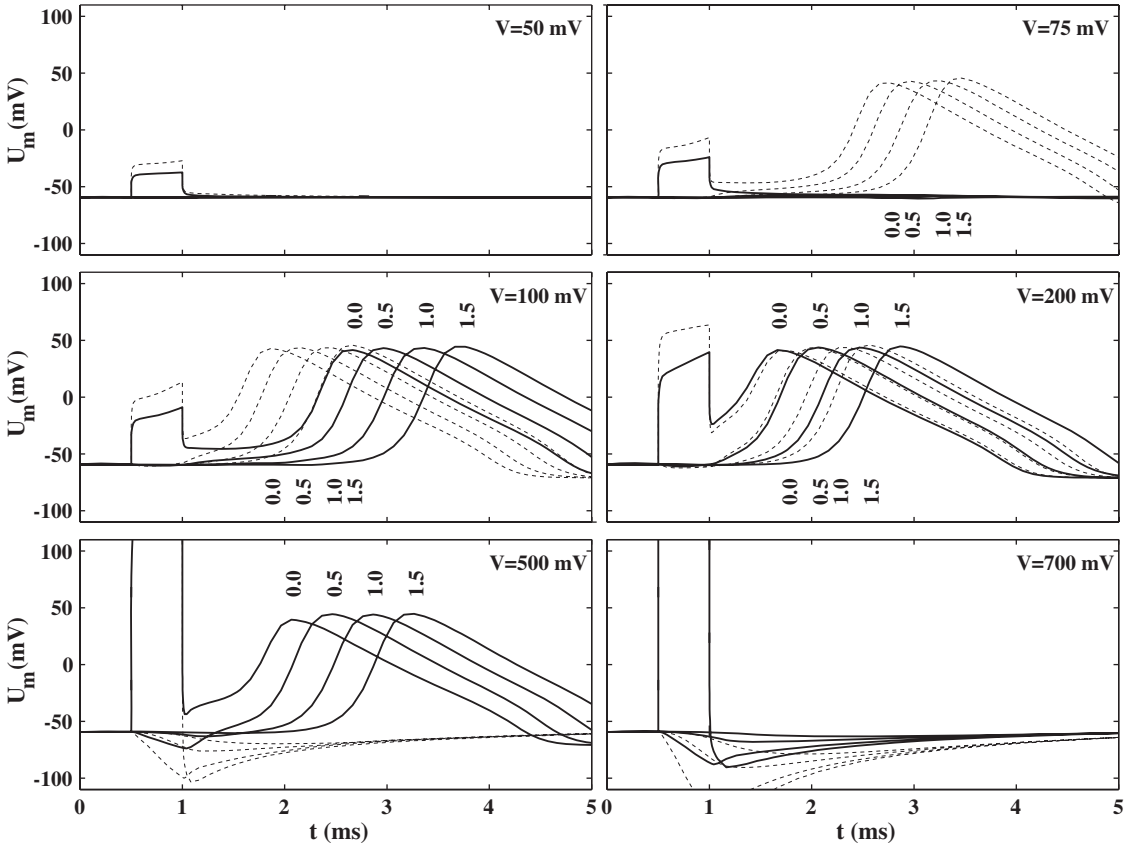

Fig. 5. Two axon response to applied electric field pulses. A 0.5 ms square voltage pulse stimulus ranging from 50 to 1500 mV (top of each panel) was applied to the two idealized (zero overvoltage) electrodes located on the sides of the system model. The dotted plots are the responses of the larger axon; the solid plots the smaller axon.

how the action potential response of the two axons varies with the stimulus amplitude. The pulses begin at $t=0.5$ ms and end at $t=1$ ms. The dotted lines are $U_m(z,t)$ for the large axon and the solid lines are the $U_m(z,t)$ for the small axon as functions of time for several slices in z. At 50 mV, there is no action potential: both transmembrane potentials remain at the level of the resting potential (−59 mV). As the amplitude is increased to 75 mV, the large axon begins to respond with an action potential. The peaks of the action potentials are labeled for each slice in z in units of millimeters. The labels below the lines are for the large axon and the labels above the lines correspond to the small axon response. The large axon should be more sensitive to the applied field because the transmembrane voltage of an isolated passive cylindrical cell changes in response to an applied electric field as

$$U_m = 2E\, r_a \cos(\theta)(1-e^{-t/\tau_m}) \quad (1)$$

$$\tau_m = 2 r_a C_m \rho_e \quad (2)$$

where E is the applied electric field amplitude, r_a is the cylinder radius, θ is the angle from the direction of the E field, t is time, τ_m is the membrane charging time, C_m is the membrane capacitance per unit area, and ρ_e is the electrolyte conductivity [24]. This expression only approximates the initial axon response of this model because of discretization limitations (square axon cross section rather than circular), the proximity to the boundary and the other axon, the electric field is not applied uniformly across the volume but rather only at $z=0$, and the non-linearity of membrane response even for sub action potential stimuli. The charging times are 0.07 and 0.14 μs for the small and large axons, respectively, much too small to appear in Fig. 5. According to Eq. (1), the passive transmembrane voltage in the direction of the applied field should scale roughly as $U_m \sim 0.17 \times V$ for the small axon and $U_m \sim 0.33 \times V$ for the large axon, which is roughly consistent with the U_m response at $z=0$ during the stimulus (0.5 ms$<t<$1 ms) before the action potential begins.

The series of dotted and solid lines show the action potential waveform as it travels away from the stimulus. As the stimulus amplitude is further increased to 100 mV, the small axon (solid lines) begins to show an action potential. By 500 mV, the large axon's action potential is quenched, while the small axon continues to respond with an action potential. At 700 mV, neither axon shows a clear action potential. The transmembrane potential is driven to negative polarity by the largest applied electric fields. This appears to be a consequence of the E field intercepting the axon membrane on both sides of the axon and the membrane response of the side with negative polarity dominates the action potential. As the applied electric field amplitude increases beyond the levels that stimulate action potentials in this system volume, there remains the possibility that fringe fields could trigger action potentials farther from the electrodes. This effect was not investigated here.

The propagating waveform shapes and amplitudes of Fig. 5 are consistent with the waveforms of Fig. 4. The action potential propagation velocities are 1.27±0.02 m s^{-1} (small axon) and 1.74±0.02 m s^{-1} (large axon), which scale with the expected dependence on axon radius ($v \sim \sqrt{r_a}$). The smaller axon's propagation velocity is somewhat faster than the 1.20 m s^{-1} for same radius axon in the system model of Fig. 4. The only differences in the small axon models are the stimulus (E field pulse vs. current clamp), the proximity to the volume boundaries, and possible interactions between the two axons. The effects of possible interactions can be isolated by removing the large axon from the model of Fig. 3 and comparing the small axon response. The action potential waveform and propagation velocity are unchanged for the small axon, but the applied field threshold is increased by ~10% in the absence of the larger axon (data not shown). The effect of the confinement volume can be isolated by applying an electric field pulse across the axon of Fig. 1 rather than using a current clamp. Once again, the waveform and propagation velocities is 1.20±0.02 m s^{-1}, but the effective electric field threshold to stimulate an action potential is significantly larger, from about 12.5 V cm^{-1} from Fig. 5 to at least 50 V cm^{-1} for the single axon in the confined volume of Fig. 1 exposed to an applied electric field at $z=0$ (results not shown). The system models of Figs. 1 and 3 are equivalent to a stack of many volumes containing parallel axons spaced in a regular pattern, all exposed to the same electric field. The packing density of the axons depends on the cross sectional area of the system model volume ($[N_x-1]\Delta_x \times ([N_y-1]\Delta_y$). The effect of packing density on passive membrane response is well known [24,30,31] and it is not surprising that active membrane response also depends on axon packing density.

This initial report demonstrates an approach to creating and solving three dimensional models that are based on an approximate system geometry on the scale of axons or nerves and also the electrodes which provide electrical stimulation. These initial results from coarse models demonstrate a new approach to describing axons. With the addition of myelinated regions it may be possible to create similar models of small but different diameter myelinated nerves in bundles.

A variety of electrode sizes, shapes and electrical properties (e.g. interfacial resistance and capacitance, half-cell potentials) can be added with greater spatial resolution than is shown here. Cylindrical axons within a nerve fiber bundle could be better represented using a meshed lattice [24] rather than the Cartesian lattice used here. This may offer the possibility of partial assessment of stimulus conditions that include important features of experimental exposures, including injurious, and therapeutic responses.

More refined local membrane models can replace or augment the HH model. The transport lattice modeling approach is modular and flexible, which allows for the prospect of creating axon membrane models with other non-linear behavior such as electroporation, through assignment of a local membrane electroporation model [23] to the axon membrane. This would allow investigation of both irreversible [32] and reversible [33] electroporation that may be spatially distributed over an axon or nerve. This is relevant to the important problem of electrical injury, in which long cells such as nerve cells are preferentially affected [34,35]. Such models may also allow investigation of various waveforms used in neuromuscular incapacitation

("stunning") [36,37], to assist in finding stimulus conditions that minimize the potential for side effects.

Acknowledgments

We thank T.F. Weiss, Z. Vasilkoski, K.C. Smith, S.N. Gozani, D.F. Freeman, and A.T. Esser for discussion and comments, and K.G. Weaver for computer support. Supported by NIH grant RO1-GM63857.

References

[1] T.F. Weiss, Cellular biophysics, Electrical properties, vol. 2, MIT Press, Cambridge, MA, 1995.
[2] D.J. Aidley, The Physiology of Excitable Cells, 4th ed. Cambridge University Press, Cambridge, 1998.
[3] I. Segev, M. London, Untangling dendrites with quantitative models, Science 290 (2000) 744–750.
[4] J.R. Buitenweg, W.L.C. Rutten, E. Marani, Extracellular stimulation window explained by a geometry-based model of the neuron–electrode contact, IEEE Trans. Biomed. Eng. 49 (2002) 1591–1599.
[5] J.R. Buitenweg, W.L.C. Rutten, E. Marani, Geometry-based finite-element modeling of the electrical contact between a cultured neuron and a microelectrode, IEEE Trans. Biomed. Eng. 50 (2003) 501–509.
[6] N.A. Trayanova, C.S. Henriques, R. Plonsey, Limitations of approximate solutions for computing the extracellular potential of single fibers and bundle equivalents, IEEE Trans. Biomed. Eng. 37 (1990) 22–35.
[7] E.N. Warman, W.M. Grill, D. Durand, Modeling the effects of electric fields on nerve fibers: determination of excitation thresholds, IEEE Trans. Biomed. Eng. 39 (1992) 1244–1254.
[8] F. Rattay, M. Aberhamm, Modeling of axon membranes for functional electrical stimulation, IEEE Trans. Biomed. Eng. 40 (1993) 1201–1209.
[9] R. Hoekema, K. Venner, J.J. Struijk, J. Holsheimer, Multigrid solution of the potential field in modeling electrical nerve stimulation, Comput. Biomed. Res. 31 (1998) 348–362.
[10] R. Rattay, Analysis of the electrical excitation of CNS neurons, IEEE Trans. BME 45 (1998) 766–772.
[11] R.G. Pay, C.D. Woody, Changes in potentiation and timing of sensorimotor transmission after adaptation of a postsynaptic transient outward current in a simulated cortical neuron, Somatosens. Motor Res. 18 (2001) 40–49.
[12] C. McIntyre, W.M. Grill, Extracellular stimulation of central neurons: influence of stimulus waveform and frequency on neuronal output, J. Neurophysiol. 88 (2002) 1592–1604.
[13] B. Bunow, I. Segev, J.W. Fleshman, Modeling the electrical behavior of anatomically complex neurons using a network analysis program: excitable membrane, Biol. Cybern. 53 (1985) 41–56.
[14] I. Segev, J.W. Fleshman, J.P. Miller, B. Bunow, Modeling the electrical behavior of anatomically complex neurons using a network analysis program: passive membrane, Biol. Cybern. 53 (1985) 27–40.
[15] H.R. Luscher, J.S. Shiner, Computation of action potential propagation and presynaptic bouton activation in terminal arborizations of different geometries, Biophys. J. 58 (1990) 1377–1388.
[16] H.R. Luscher, J.S. Shiner, Simulation of action potential propagation in complex terminal arborizations, Biophys. J. 58 (1990) 1389–1399.
[17] M. Bove, G. Massobrio, S. Martinoia, M. Grattarola, Realistic simulations of neurons by means of an ad hoc modified version of SPICE, Biol. Cybern. 71 (1994) 137–145.
[18] M. Grattarola, S. Martinoia, Modeling the neuron–microtransducer junction: from extracellular to patch recording, IEEE Trans. BME 40 (1993) 35–41.
[19] M. Grattarola, M. Bove, S. Martinoia, G. Massobrio, Silicon neuron simulation with SPICE: tool for neurobiology and neural networks, Med. Biol. Eng. Comput. 33 (1995) 533–536.
[20] R. Weis, B. Müller, P. Fromherz, Neuron adhesion on a silicon chip probed by an array of field-effect transistors, Phys. Rev. Lett. 76 (1996) 327–330.
[21] R. Weis, P. Fromherz, Frequency dependent signal transfer in neuron transistors, Phys. Rev., E Stat. Phys. Plasmas Fluids Relat. Interdiscip. Topics 55 (1997) 877–889.
[22] T.R. Gowrishankar, J.C. Weaver, An approach to electrical modeling of single and multiple cells, Proc. Natl. Acad. Sci. 100 (2003) 3203–3208.
[23] D.A. Stewart, T.R. Gowrishankar, J.C. Weaver, Transport lattice approach to describing cell electroporation: use of a local asymptotic model, IEEE Trans. Plasma Sci. 32 (2004) 1696–1708.
[24] D.A. Stewart, T.R. Gowrishankar, K.C. Smith, J.C. Weaver, Cylindrical cell membranes in uniform applied electric fields: validation of a transport lattice method, IEEE Trans. Biomed. Eng. (2005) 1643–1653.
[25] T.R. Gowrishankar, D.A. Stewart, and J.C. Weaver. Model of a confined spherical cell in uniform and heterogeneous applied electric fields. Bioelectrochemistry (in press).
[26] A.L. Hodgkin, A.F. Huxley, A quantitative description of membrane current and its application to conduction and excitation in nerve, J. Physiol. 117 (1952) 500–544.
[27] T.F. Weiss. Cellular Biophysics: Teaching and Learning with Computer Simulations. http://umech.mit.edu/6.021J/2003/manual5.pdf, 2000.
[28] D.C. Mikulecky, Applications of network thermodynamics to problems in biomedical engineering, New York University Press, New York, 1993.
[29] A. Vladimirescu, The SPICE book, John Wiley and Sons, New York, 1994.
[30] R. Susil, D. Semrov, D. Miklavĉiĉ, Electric field induced transmembrane potential depends on cell density and organization, Electro. Magnetobiol. 17 (1998) 391–399.
[31] M. Pavlin, N. Pavselj, D. Miklavĉiĉ, Dependence of induced transmembrane potential on cell density, arrangement, and cell position inside a cell system, IEEE Trans. Biomed. Eng. 49 (2002) 605–612.
[32] R. Stämpi, M. Willi, Membrane potential of a Ranvier node measured after electrical destruction of its membrane, Experientia 8 (1957) 297–298.
[33] R. Stämpi, Reversible electrical breakdown of the excitable membrane of a Ranvier node, An. Acad. Bras. Cienc. 30 (1958) 57–63.
[34] R.C. Lee, M.S. Kolodney, Electrical injury mechanisms: electrical breakdown of cell membranes, Plast. Reconstr. Surg. 80 (1987) 672–679.
[35] R.C. Lee, D. Zhang, J. Hannig, Biophysical injury mechanisms in electrical shock trauma, Ann. Rev. Biomedical. Eng. 2 (2000) 477–509.
[36] R.M. Fish, L.A. Geddes, Effects of stun guns and tasers, Lancet 358 (2001) 687–688.
[37] W.C. McDaniel, R.A. Strabucker, M. Nerheim, J.E. Brewer, Cardiac safety of neuromuscular incapacitating defensive devices, Pacing Clin. Electrophysiol. 28 (Suppl. 1) (2005) S284–S287.